Rational Selection of Gold Nanorod Geometry for Label-Free Plasmonic Biosensors

Greg J. Nusz, Adam C. Curry, Stella M. Marinakos, Adam Wax, and Ashutosh Chilkoti*

Department of Biomedical Engineering, Duke University, Durham, North Carolina 27708

ABSTRACT We present the development of an analytical model that can be used for the rational design of a biosensor based on shifts in the local surface plasmon resonance (LSPR) of individual gold nanoparticles. The model relates the peak wavelength of light scattered by an individual plasmonic nanoparticle to the number of bound analyte molecules and provides an analytical formulation that predicts relevant figures-of-merit of the sensor such as the molecular detection limit (MDL) and dynamic range as a function of nanoparticle geometry and detection system parameters. The model calculates LSPR shifts for individual molecules bound by a nanorod, so that the MDL is defined as the smallest number of bound molecules that is measurable by the system, and the dynamic range is defined as the maximum number of molecules that can be detected by a single nanorod. This model is useful because it will allow *a priori* design of an LSPR sensor with figures-of-merit that can be optimized for the target analyte. This model was used to design an LSPR sensor based on biotin-functionalized gold nanorods that offers the lowest MDL for this class of sensors. The model predicts a MDL of 18 streptavidin molecules for this sensor, which is in good agreement with experiments and estimates. Further, we discuss how the model can be utilized to guide the development of future generations of LSPR biosensors.

KEYWORDS: nanoparticle · plasmonics · label-free · biosensor · surface plasmon resonance · limit-of-detection · gold nanorods

The unique optical properties of plasmonic nanoparticles have led to the development of a novel class of label-free biomolecular sensors. These biosensors exploit the phenomenon of localized surface plasmon resonance (LSPR) which endows unique light scattering and absorption properties to noble metal nanoparticles that are a function of the local environment. This behavior transduces binding events at the nanoparticle surface into a macroscopically measurable optical signal[1−6] and forms the basis of LSPR biosensors. Herein, we report the derivation and experimental verification of an analytical model that predicts the figures-of-merit of nanoparticle LSPR biosensors operating at the single particle limit and provides guidance for the rational design of LSPR biosensors.

LSPR arises from the resonant oscillation of conduction electrons on the surface of metal nanoparticles. The energy associated with this resonance is a function of the nanoparticle composition, size, shape, and the surrounding dielectric environment.[7−12] Noble metal nanoparticles with features in the 10−100 nm size scale exhibit plasmonic resonances at optical frequencies. Consequently, such nanoparticles exhibit a characteristic LSPR spectrum, with one or more peaks in the visible light range that correspond to specific electron oscillation resonances. The LSPR peak location and intensity are sensitive to the local refractive index (RI) surrounding the nanoparticle and are the basis of their utility as biosensors. Binding of analyte molecules to nanoparticles that are decorated with a receptor specific for that analyte alters the local RI in the vicinity of the plasmonic nanostructure, resulting in a shift of the LSPR spectrum. This shift can be measured either as a change in the peak intensity of the scattered light or as a shift in the LSPR peak wavelength (λ*).

This approach to biomolecular detection was initially proposed for plasmonic particles in suspension,[13] was then demonstrated for an ensemble of gold nanoparticles that were immobilized on a transparent substrate in a chip-based format by our group,[14,15] and was subsequently validated by other groups[16−18] and extended to the limit of single nanoparticles.[5,19−25] By miniaturizing the sensor down to a single nanoparticle, the detection system is reduced to the size-scale that is commensurate with the size of biomolecular analytes. To further understand the mechanics of single-nanoparticle detection, investigators have also been studying the specific details of plasmonic nanostructures that are responsible for their use in sensors such as the distance dependence of sensitivity[26−28] and the resonant electric field enhancement distribution.[29,30] However, to date, these

*Address correspondence to chilkoti@duke.edu.

Received for review October 2, 2008 and accepted March 09, 2009.

Published online March 18, 2009.
10.1021/nn8006465 CCC: $40.75

developments have not been integrated into a coherent quantitative framework that allows the effect of these parameters on relevant figures-of-merit of biosensors, such as their limit of detection and dynamic range, to be predicted.

Motivated by the goal of rationally designing LSPR sensors, in this paper, we integrate recent progress in understanding the structural details of metal nanoparticles that control their plasmonic behavior with various measurement system parameters that impact measurement uncertainty into a quantitative model that is capable of predicting the response of a single, receptor-functionalized nanoparticle to discrete analyte binding events. The result is an analytical model that quantifies the LSPR shift of a gold nanorod caused by the local refractive index increase from the presence of a target biomolecule. The principle of this work is similar to that of Stemberg *et al.* who describe an analytical model to quantify the surface concentration of bound protein on plasmon resonant planar gold[31] and to that of Vollmer *et al.* who estimate the surface density of bound proteins based on wavelength shifts of a resonant microcavity.[32]

The utility of this model is two-fold. First, it provides an analytical model that allows *a priori* design of an LSPR sensor with figures-of-merit, such as the molecular detection limit (MDL) and dynamic range, that can be analytically calculated completely as a function of sensor components for a given receptor−analyte pair. Because the model calculates LSPR shifts for individual bound molecules, the MDL is defined as the smallest number of bound molecules that is measurable by the system, and the dynamic range is the maximum number of detectable molecules. To illustrate its experimental utility, the model was used to identify the optimal gold nanorod geometry (length and diameter) that was predicted by the model to yield the lowest MDL for the detection of streptavidin by gold nanorod LSPR sensors. An LSPR sensor was fabricated from biotin-functionalized gold nanorods, and the experimental results were compared with the prediction of the model to investigate its accuracy. Second, this model is useful because it allows the contribution of different system parameters to overall sensitivity to be individually parsed. With the ultimate goal of label-free, single molecule detection by LSPR sensors, we conclude with a discussion of optimization of the system within realistic physical and current technological constraints that might allow the fabrication of an LSPR sensor and dark-field microspectrometer that are capable of detecting the binding of individual analyte molecules.

RESULTS AND DISCUSSION

As a first approximation, the MDL of nanoparticle sensors is determined by their composition, size, and shape of the NPs. Recognizing that the development of a generalized model that could account for the dependence of the MDL of an LSPR sensor on all of these parameters was likely to prove computationally intensive and possibly intractable, we focused instead on developing a model that was applicable to gold nanorods as plasmonic transducers of binding events for the following reasons. First, although silver particles are more sensitive than gold particles of the same shape and size,[33] the greater reactivity of silver as compared to gold makes it less suitable for use in biologically relevant media as silver can be easily oxidized, altering the plasmonic behavior of the particle. Second, gold nanorods can be conveniently synthesized with a range of dimensions *via* established chemical synthesis methods, which allows the model to be experimentally tested—and the sensor optimized—at the structural level.[34−36] Third, gold nanorods can be conveniently synthesized to exhibit plasmon resonances with peak wavelengths ranging from 700 to 900 nm and beyond simply by tuning their aspect ratio and size.[34,37−40] This spectral region is particularly useful for biosensing because the background absorption and scattering of endogeneous chromophores from biological mixtures (*e.g.*, serum and blood) and of water are minimal in this wavelength range.[41,42] We note that LSPR of several other geometries of gold nanoparticles such as nanoshells, nanodiscs,[43] and nanorings[44] can also be tuned *via* synthesis methods to exhibit plasmon bands in the wavelength range of gold nanorods. Nanorods, however, have a higher bulk RI sensitivity[45] and also a narrower line width than these geometries,[43,44,46] which allows more accurate determination of peak shifts as described later in the model details. Additionally, the line widths of gold nanorod scattering spectra have been shown to be a function of the length and aspect ratio of the gold nanorods[47] as well as end-cap shape,[48] parameters that can be controlled in their chemical synthesis.

Model Development. We sought to develop an analytical model that estimates the MDL of an LSPR sensor for a specific analyte−receptor pair based on the geometric dimensions of the gold nanorod using a specified spectral detection system. Thus, the model is an equation that predicts the minimum number of detectable analyte molecules based on input parameters that consist of the nanorod dimensions and optical system parameters. Building the model involved several steps; first, the spectral detection system and data analysis algorithms were analyzed to determine the measurement uncertainty in detecting LSPR peak wavelengths. Then, the average number of analyte molecules that must bind to induce an LSPR shift equal to the measurement uncertainty for a given nanorod geometry was determined. This is the smallest number of bound molecules that can be reliably be detected by the proposed system and is defined as its MDL. It is important to note that we define the MDL by the amount of material bound to the surface of the nanoparticle,

and not the concentration of the analyte in the surrounding medium. This choice was made so that the focus of the model is the interaction of the bound analyte with the plasmonic nanoparticles and the subsequent LSPR signal generated, and not the mass transport kinetics of the sensor system. Therefore, the optimal nanoparticle can be determined for a proposed analyte strictly by using the model to predict which geometry will offer the lowest MDL.

The first step in the derivation of the model was estimation of the minimum LSPR shift that can be reliably measured for a particular detection system. We assumed that the total uncertainty is the sum of uncertainties induced by two factors as represented in eq 1: uncertainty introduced by the detection system, U_{system}, and uncertainty introduced by the peak fitting to the gathered nanoparticle scattering spectrum, U_{fit}.

$$U = \sqrt{U^2_{system} + U^2_{fit}} \quad (1)$$

A thorough discussion of the U_{system} of the microspectroscopy system utilized in this work has been reported elsewhere.[49] That study, which incorporated considerations of image focus, physical sample stability, and overall repeatability of the measurements, concluded that U_{system} was ~0.3 nm for the optical detection system described in that work. The same experimental setup was used in this study; hence we assume that U_{system} is 0.3 nm.

Next, uncertainty due to the data analysis method must be considered. The measurement noise was modeled as a Gaussian distribution. Although the physical model of noise in an optical measurement is a Poisson distribution due to shot noise, it can be accurately and conveniently modeled by a Gaussian distribution for a large number of photons because it is merely a counting problem. This yields the following relationship for U_{fit}

$$U_{fit} = \frac{1}{2}\frac{FWHM}{2.35 \cdot SNR} \quad (2)$$

where FWHM is the line width of the spectrum being fit and SNR is the signal-to-noise ratio of the data being fit.[49] The SNR depends on photoelectron signal magnitude, M, the integration time, t, and the spectrometer camera's dark current specification, N_d, and read noise, N_r, according to the following:

$$SNR = \frac{M}{\sqrt{M + N_d t + N_r^2}} \quad (3)$$

For a shot noise-limited measurement ($SNR = \sqrt{M}$), the shot noise dominates over the dark and read noise. The system used for this study has a dark current of less than 0.0025 electrons $\cdot$ pixel$^{-1} \cdot$ s^{-1} and read noise of less than 4 electrons RMS such that a shot noise-limited measurement (defined here as a measurement for which shot noise exceeds dark and read noise sources by an order of magnitude) will have an SNR > 13 for a typical integration time of 20 s. The role of the nanoparticle geometry in affecting measurement uncertainty becomes apparent as the signal level; that is, the amount of light scattered is proportional to the nanoparticle's scattering cross section, C_{sca}. Thus in the shot noise-limited regime, the following relationship holds for SNR:

$$SNR_{SNL} = \sqrt{M} = \sqrt{A \cdot C_{sca}} \quad (4)$$

where A is a constant that accounts for the input photon flux, the integration time, and the quantum efficiency of the measurement system. The parameter A can be calculated for a microspectroscopy system by making a shot noise-limited measurement of the SNR of a nanoparticle with known C_{sca}.[50] We measured the scattering spectrum of an 80 nm diameter gold sphere under typical operating parameters and observed a SNR of 100. Using the C_{sca} predicted by Mie theory of the sphere, a value of 0.385 is determined for A for the microspectroscopy system described in this work. With the value for A known, the SNR for an arbitrary nanoparticle of known C_{sca} may be calculated by rewriting eq 7 as follows:

$$SNR = \frac{A \cdot C_{sca}}{\sqrt{A \cdot C_{sca} + N_d t + N_r^2}} \quad (5)$$

Now, with eqs 2 and 5, it is possible to calculate total peak measurement uncertainty for an arbitrary particle based on the FWHM and C_{sca} of the particle, even if the measurement is not shot noise-limited. C_{sca} can be determined analytically as a function of nanorod geometry by applying the model developed by Kuwata *et al.*[51] Further details of the specific application of this model are reported below. Therefore, U can now be calculated entirely as a function of nanorod length and diameter. It is worth noting that the constant A is dependent upon the measurement system, but not upon the measured nanoparticle. Thus, it must only be empirically determined once for a specific experimental setup.

The next step in the development of the model was to analytically translate this uncertainty limit from units of wavelength shift to number of bound molecules as a function of nanorod geometry. In order to formulate this relationship in a manner that is analytically simple, several approximations and assumptions were made. First, we assumed that the nanorods are cylindrical in shape with a length (l) and diameter (d). We recognize that the assumption that the nanorods are perfect cylinders is an approximation because transmission electron microscopy (TEM) images of chemically synthesized nanorods indicate that the nanorods are only approximately cylindrical, as they have "end-caps" with visible curvature on their ends. This approximation will introduce some error as it has been shown that

end-cap geometry has an impact on the optical scattering spectra of nanorods.[48,52] We also assumed that the LSPR peak shift, $\Delta\lambda_{LSPR}$, resulting from a bound analyte is proportional to the total LSPR shift that is expected if the entire surrounding medium increased to the RI of the analyte. The proportionality constant is the ratio of the analyte volume to the total sensing volume of the nanorod. This assumption yields the following relationship:

$$\frac{\Delta\lambda_{LSPR}}{\Delta RI \cdot S(r)} = \frac{V_D}{V_S} \quad (6)$$

where V_S is the total sensing volume of the nanorod, V_D is the volume of the detected analyte, $S(r)$ is the spatially dependent RI sensitivity of the nanoparticle, and r is the distance of the bound molecule from the surface of the nanorod. Because the RI sensitivity decreases away from the nanoparticle surface, the sensing volume is defined as the fixed volume surrounding the nanorod that contains 95% of its sensitivity. Recognizing that the optical mass of the bound molecules is responsible for inducing the observed LSPR shifts, the optical mass increase induced by bound analyte is defined as the product $V_D \cdot \Delta RI$, where V_D is the volume of analyte bound to the nanorod and ΔRI is the difference between the RI of the analyte and that of the surrounding medium. In the case where the approximate size of the analyte is known, the detection volume V_D can be replaced with the product $N \cdot V_A$ where V_A is the volume of the analyte molecule and N is the number of bound molecules to the nanorod. Substituting this parameter in eq 6 and rearranging for $\Delta\lambda_{LSPR}$ yields an expression relating the measured peak shift of the LSPR spectrum to the optical detection mass:

$$\Delta\lambda_{LSPR} = \frac{S(r)}{V_S}\Delta RI \cdot N \cdot V_A \quad (7)$$

Solving eq 7 for N yields an expression that can be used to translate an observed LSPR peak shift into the number of bound molecules.

$$N = \frac{\Delta\lambda_{LSPR}}{\Delta RI \cdot S(r)} \cdot \frac{V_S}{V_A} \quad (8)$$

In order to determine the MDL of the system, we replace $\Delta\lambda_{LSPR}$ in eq 8 with U, the uncertainty of the optical system in detecting wavelength shifts. Thus, the right-hand side of eq 8 becomes an expression of the bound optical mass that would induce the minimum detectable LSPR wavelength shift. In this case, solving for N yields an expression for L_M, the MDL of the system in terms of the minimum detectable number of bound biomolecules.

$$L_M(l, d) = N = \frac{V_S}{V_A} \cdot \frac{U}{S(r) \cdot \Delta RI} \quad (9)$$

where L_M is a function of the length l and diameter d of the nanorod. From eq 9, we observe that the function L_M is determined by several parameters on the right-hand side. Careful examination of these parameters is required to fully understand the dependence of each on the nanorod geometry and the effect each has on the overall MDL of the system. We note that L_M is dependent upon the detection system employed for measuring the LSPR shifts of single nanoparticles because of the dependence on the peak measurement uncertainty U. L_M is also a function of the spatially dependent RI sensitivity $S(r)$ of the nanoparticle, where r is the location of the bound molecule with respect to the surface of the nanorod.

In order to determine the function L_M analytically, we next sought to define the parameters U and $S(r)$ based solely on the length and diameter of the nanorod, as follows: first, we utilized a model developed by Kuwata and co-workers to approximate the wavelength-dependent scattering cross section (C_{sca}) of gold nanorods as a function of nanorod geometry. This model provides the complete LSPR scattering spectrum of the nanorod with a simple analytical formula based on nanorod length and diameter. The model is based on fits to finite-difference time-domain with the depolarization factor calculated by electrostatic approximation.[51] We employed this formula to determine the location of the LSPR peak (λ^*) and scattering cross section C_{sca} at the peak wavelength for nanorods of arbitrary length and diameter. A second analytical model, based on Gans's extension of Mie theory that simulates LSPR spectra as a function of the nanorod aspect ratio,[53−55] was also used to simulate spectra as a means of validation. These two models provided consistent results within the geometric range of nanorods studied (length 50−100 nm and diameter 15−50 nm). These predictions were then further verified experimentally by comparison to scattering spectra of individual, chemically synthesized nanorods as shown in Figure 1. The good agreement between experimentally collected LSPR spectra and simulated spectra further indicates the utility of the analytical model.

It has been shown that LSPR shifts induced by local RI have a strong distance dependence as a result of the exponential decrease in field enhancement further from the nanoparticle surface.[26] This distance dependence of sensitivity has been experimentally measured for nanospheres[56] as well as anisotropic triangular nanoparticles.[57] Additionally, it has been shown that the LSPR associated electric field is enhanced near the ends of nanorods.[29,30] These observations suggest that the location at which a target analyte binds to the nanorod (*i.e.*, along the sides or at the ends) will affect the magnitude of the induced LSPR shift. The detector−analyte system described in this work provides reasonable certainty in estimating the average binding distance, which is determined by the length of the receptor conjugated to the nanorod (biotin in the ex-

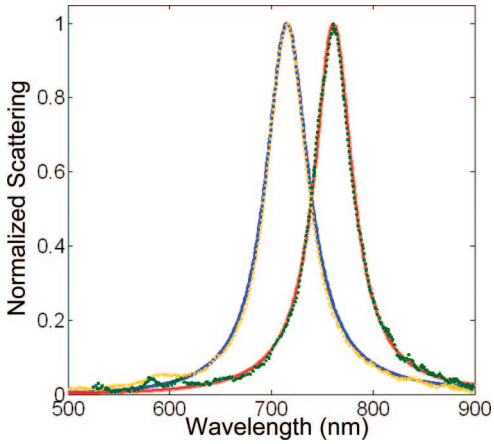

Figure 1. Comparison of simulated *versus* experimental spectra. Scattering spectra collected from single nanorods from synthesized batches characterized by TEM to be (63.3 ± 8.2) × (24.9 ± 4.9) nm (n = 319, yellow dotted line) and (74 ± 9) × (33 ± 6) nm (n > 100, green dotted line). Simulated spectra for nanorods with dimensions of 64.5 × 24.7 nm (blue line) and 75 × 32 nm (red line) *via* the Kuwata method are also shown.

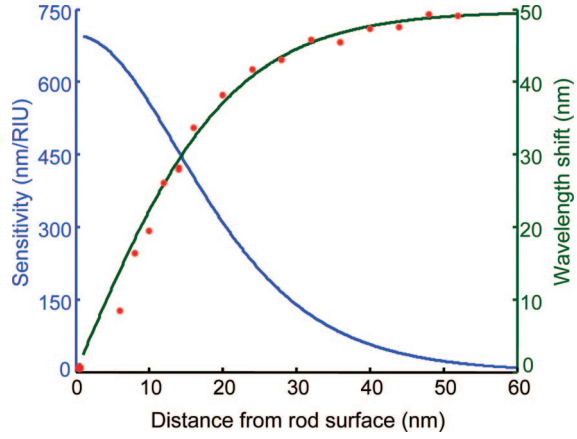

Figure 2. Right axis: experimental wavelength shift of a nanorod (63.3 ± 8.2 nm × 24.9 ± 4.9 nm) as a function of deposited polyelectrolyte thickness (red dots) and shifts predicted by eq 7 (green line). Left axis: corresponding calculated distance dependence of the nanorod LSPR sensitivity (blue line).

perimental case tested herein) and its binding site. Hence, we model sensitivity as being a function solely of the distance r from the surface of the nanorod $S(r)$. The effect of this assumption is that the model effectively outputs the LSPR response of the *average* bound analyte at a fixed distance r from the surface of the nanorod. This is a simplification of the physical phenomenon because of the known complexity of the electric field enhancement distribution. Nevertheless, this model is the closest representation to the actual detection experiments because the actual binding locations cannot be controlled nor can the fraction of analytes that bind along the nanorod ends *versus* sides be accurately estimated.

With these assumptions clarified, we sought to generate an analytical function that describes $S(r)$ purely as a function of nanorod geometry. This was accomplished by first experimentally measuring $S(r)$ for several nanorod geometries spanning the dimensions of interest. This was done by using a procedure previously reported to probe the sensing volume of gold nanospheres by adsorbing sequential layers of oppositely charged polyelectrolytes to the nanoparticle surface.[14] These experiments provided data on the dependence of $S(r)$ on nanorod geometry. These data were then curve-fit to describe $S(r)$ for nanorods of arbitrary length and diameter. From this fit, the sensing volume of the nanorod V_S and the decay length of electric field enhancement l_d were also determined as a function of nanorod geometry. V_S is defined as the fixed distance from the nanorod surface containing 95% of $S(r)$, and the decay length is the distance from the nanorod surface at which the electric field enhancement is reduced by a factor of e. Figure 2 shows the excellent agreement obtained between the model and experimental data. Details of this fitting procedure are further described in the Supporting Information. With the results of this fit, it is possible to write every parameter on the right-hand side of eq 8 as an analytical function of the length and diameter of the nanorod such that the MDL, L_M, of an arbitrary nanorod can be analytically estimated from the length and diameter of the nanorod.

$$L_M = \frac{V_S}{V_A \cdot \Delta RI} \cdot \frac{\sqrt{U^2_{system} + U^2_{fit}}}{\exp\left(\frac{-2r}{l_d}\right) \cdot (3S_0)} \qquad (10)$$

where V_S is the sensing volume, V_A is the analyte volume, ΔRI is the RI difference between the analyte and the surrounding medium, U_{system} is the peak measurement uncertainty resulting from uncertainty in the physical detection of the LSPR peak, U_{fit} is peak determination uncertainty due to data fitting, S_0 is the bulk RI sensitivity, r is the distance from the nanorod surface that the analyte binds, and l_d is the decay length of the resonant electric field.

Equation 10 is especially useful because it allows an analysis of the overall performance of a single nanoparticle based on a variety of parameters, only one of which is the nanoparticle bulk RI sensitivity S_0. We emphasize this point because much work in the field has been devoted to synthesizing nanoparticles with different geometries and compositions in order to optimize the RI sensitivity of the nanoparticle.[45,58,59] Clearly, the nanoparticle bulk sensitivity is an important contributor to the overall MDL; however, it is not necessarily the most important. In fact, Miller *et al.* have shown that the bulk RI sensitivities of nanoparticles can be predicted from the wavelength of the LSPR peak, independent of nanoparticle shape.[60,61] The parameter U is also clearly important in determining MDL but has largely been ignored on discussions of MDL.[49] Obviously the sensitivity of the detection system depends not only on the signal generated by the nanoparticles but also

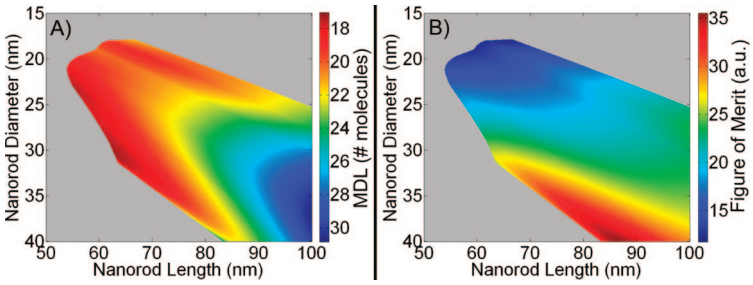

Figure 3. (A) Calculated molecular limits of detection for gold nanorods of arbitrary dimension based on eq 10. (B) Composite figures of merit (FOM) for nanorods of arbitrary dimensions. The composite FOM is calculated as the maximum number of bound molecules divided by the minimum number of detectable molecules. The surrounding gray regions in both are indicative of nanorod geometries that were not considered in this model because they either had resonances outside the visible spectrum or had scattering cross sections that are insufficient to collect spectra with SNR greater than 30.

how precisely it can be measured. This parameter is primarily dependent on optical detection system parameters and data analysis techniques. However, U also depends on nanoparticle geometry because spectra for nanoparticles with higher C_{sca} can be measured more accurately due to their increased scattering signal as seen in eq 10. Other parameters, such as the effective sensing volume of the nanoparticles (*i.e.*, the electric field enhancement localization) can vary a great deal across geometries and have a large impact on the sensing characteristics of a nanoparticle. Nanoparticles with more confined electric field enhancements maintain smaller sensing volumes, resulting in larger shifts upon analyte binding within the sensing volume. However, nanoparticles with smaller detection volumes have a smaller dynamic range because they saturate upon the binding of fewer analytes. The proposed model offers a means to collectively analyze the effects of these parameters on overall sensor performance to deduce the optimal nanoparticle geometry for an LSPR sensor that is designed for a specific application.

Figure 3A shows the theoretical MDL for streptavidin binding to biotin decorated gold nanorods as predicted by eq 10 for single nanorods of arbitrary dimensions when measured in the described microspectroscopy system for which U has been previously characterized. We chose this analyte−receptor pair because their interaction is one of the best characterized and most commonly used model receptor−analyte systems. The simulation was restricted to nanoparticles that have LSPR peak wavelengths in the range of 300−900 nm because that is the range observable in the microspectroscopy system. We also applied a minimum SNR threshold of 30 to exclude particles with small C_{sca} that cannot produce enough scattered light to be visualized in the dark-field microscopy setup. For this reason, no data are shown for nanorods with LSPR peaks outside of this range or with SNR below the cutoff of 30. We assumed the streptavidin molecules have a volume[62] of 114 nm^3 and RI of 1.57.[63] From Figure 3A, we can see that nanorods with lengths between 55 and 65 nm and diameters between 25 and 33 nm offer the lowest MDL of ~18 streptavidin molecules. It is important to note that the nanorod MDLs predicted by eq 10 are a monotonic function of several detection system and analyte parameters. Although the absolute value of the MDL will vary across detection systems and receptor−analyte pairs, the relative performance of a nanorod with a specified geometry will not vary, so that once the optimal rod geometry has been identified for a target analyte it will always offer the lowest MDL across detection systems and receptor−ligand configurations.

In addition to the absolute MDL, the dynamic range (DR) is an important figure-of-merit (FOM) of a biomolecular sensor. For the purposes of this model, the DR is defined as the theoretical maximum number of analyte molecules that are detectable by a single nanorod. This definition was chosen because it is consistent with the model output, which is quantified as the number of bound molecules. The DR was determined by calculating the total surface area available for binding and dividing it by the footprint of a bound analyte molecule. This value was then scaled by a factor of 0.9, which assumes a hexagonal packing density of hard spheres yielding the highest possible coverage that could be achieved in practice. By this definition, a larger nanorod will obviously exhibit a higher DR because of its larger surface area. However, larger nanorods also tend to have higher MDLs because of the increased sensing volume. To balance these considerations, we calculate a composite FOM for nanorods that includes both the DR and MDL of these nanorod plasmonic sensors operating in the single nanorod mode. The composite FOM is calculated simply as the ratio of the DR *versus* its MDL. Figure 3B shows the composite FOM for nanorods of arbitrary dimensions. Figure 3B shows that rods with a length of 85 nm and a diameter of 40 nm offer the highest composite FOM with the potential to bind ~35 times as many molecules as is required to generate its lowest detectable signal. So although nanorods of those dimensions may exhibit a MDL of ~22, their higher dynamic range indicates they may be more useful as a streptavidin sensor over a wider range of analyte concentrations.

Experimental Application of Model. To experimentally test the results provided by the model, gold nanorods were synthesized with dimensions that were as close to the geometry predicted by eq 9 (and visually represented by Figure 3A) to have the lowest streptavidin MDL. To experimentally test the predictions of the model, streptavidin binding experiments were performed using biotin-functionalized gold nanorods that were shown by TEM to have a length of 63.3 ± 8.2 nm and a diameter of 24.9 ± 4.9 nm (n = 319) (Figure 4). Equation 10 calculates that these rods have a mean MDL of 20 molecules and mean FOM of 22.

A dose−response curve was determined by incubating identical samples of biotin-functionalized gold nanorods that were chemisorbed on glass slides in streptavidin solutions that spanned a range of protein concentration. Figure 4 (right panel) shows the steady-state LSPR shift of single nanorods as a function of streptavidin concentration. A sigmoidal fit was applied to these data, and the concentration at which the fit crosses the LSPR peak measurement uncertainty of 0.3 nm was defined as the experimental detection limit. For the experiments shown in Figure 4, the detection limit is 160 pM.

To investigate the relationship between the experimental detection limit measured by analyte concentration and the MDL predicted by eq 10, we specifically looked at the detection of 100 pM streptavidin. Figure 5 shows fits to scattering spectra collected from a single nanorod incubated in 100 pM streptavidin. The blue line is the nanorod LSPR scattered spectrum in water, the red line is the spectrum after the binding of biotin, and the black line is the spectrum after incubation in 100 pM streptavidin. The ~3 nm shift between the blue and green lines observed upon biotin functionalization is consistent with the adsorption of a thin dielectric layer. The length of the biotin−amine is estimated to be 2.39 nm (Chem3d, Cambridgesoft) and the SAM to which the biotin is conjugated has a thickness of 2.78 nm and RI of 1.464.[64] Using eq 6 to simulate the LSPR response of the addition of dielectric layers yields an expected LSPR peak shift of 3.59 nm. This value is in good agreement with the experimental mean LSPR shift of 3.23 ± 1.2 nm observed upon the incubation of biotin for all nanorods used in the streptavidin detection experiments.

A 0.52 nm shift was observed upon incubation of the biotin-functionalized gold nanorods in 100 pM streptavidin, which translates to ~27 streptavidin molecules bound by a single nanorod, by use of eq 8. Lower streptavidin concentrations were tested in order to establish the detection limit in terms of concentration but did not yield results that were statistically significant from negative control experiments,[19] so the lowest streptavidin concentration that was experimentally detected is 100 pM. This experimentally detected minimum of approximately 27 molecules is reasonably close to the theoretical MDL of 20 streptavidin molecules per nanorod predicted by the model for the nanorods used. Thus, by utilizing the proposed model (eq 10), specifically, to select the optimal nanorod geometry for streptavidin detection, we are able to observe binding in the picomolar range. To our knowledge, this is the lowest reported concentration of biomolecule detected with a single particle LSPR sensor.

As a further check of the relevance of the MDLs predicted by our model, we observed that the mean LSPR shift at saturation is 5.4 nm (Figure 4). Using eq 8, we calculate that this shift arises from the binding of approximately 280 streptavidin molecules to the nanorod surface. For the nanorods used in these experiments, approximately 8000 nm^2 of biotin-activated surface is available for the binding of streptavidin molecules. Each streptavidin molecule is a tetramer of four identical biotin binding subunits, and the entire tetramer is roughly ellipsoidal with axes of 5.4 nm × 5.8 nm × 4.8 nm.[65,66] Thus, the footprint that a streptavidin molecule would occupy on the binding surface is approximately 25 nm^2. In this orientation, a maximum of only 320 molecules would be expected to fit on the nanorod surface. Approximating the streptavidin molecules as hard spheres, the model of random sequential adsorption[67] predicts a packing ratio of 0.54, which would translate to only 170 bound molecules, whereas the highly ordered method of hexagonal packing predicts a packing ratio of 0.9, allowing for up to 290 streptavidin molecules. Therefore, the 280 molecules bound at saturation as determined by eq 8 is reasonable and suggests a more ordered arrangement of bound streptavidin molecules.

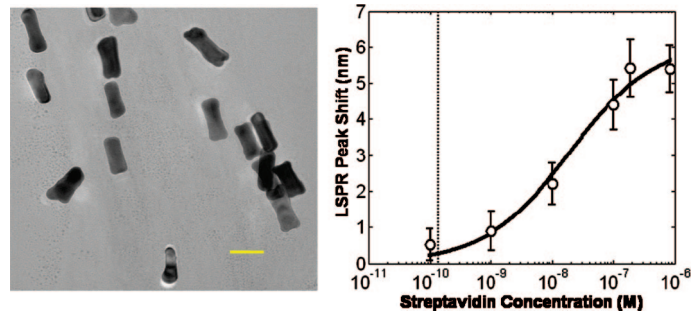

Figure 4. Left: TEM of rods used in this study. Nanorod length is measured to be 63.3 ± 8.2 nm and diameter 24.9 ± 4.9 nm (n = 319). Scale bar corresponds to 50 nm. Right: LSPR peak shift of individual, biotin-activated gold nanorods *versus* concentration of streptavidin. Open circles are the mean LSPR shift of approximately 15 nanorods per measurement at each concentration, and the error bars indicate 95% confidence interval. The solid line is a sigmoidal fit to the data. The dotted line indicates where the fit line crosses 0.3 nm shift, the measurement detection uncertainty as calculated above. This occurs at a concentration of 160 pM.

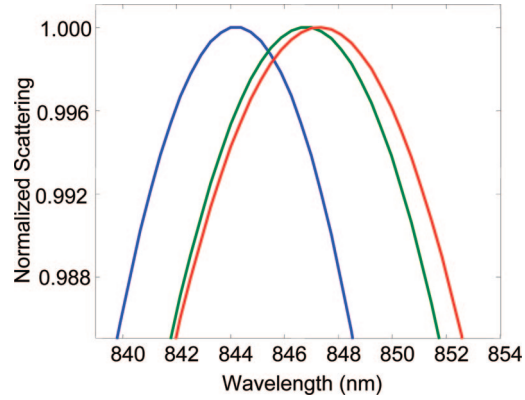

Figure 5. Fits to scattering spectra of a single nanorod in water (blue), after biotin conjugation (green), and subsequently in 100 pM streptavidin (red). The 0.52 nm shift corresponds to approximately 27 streptavidin molecules by eq 8.

Additionally, we compare the mass of streptavidin presumed bound at saturation by eq 8 with that of streptavidin adlayers that were experimentally measured. Densities of 240 and 231 ng/cm^2 have been experimentally determined for streptavidin layers formed over biotin layers on flat substrates.[68,69] These binding densities yield an estimated ~220 bound streptavidin molecules to the available nanorod binding area of 8000 nm^2. Again, these estimates are slightly lower than the 280 molecules estimated from eq 8 to be responsible for the 5.29 nm shift observed at saturation but are close enough to justify the validity of our calculations.

Prospects for Single Molecule Detection. We systematically explored the parameters in eq 10 within physically realistic limits to determine which parameters can be modified in order to develop an LSPR sensor with a single molecule MDL.

The product $V_A \cdot \Delta RI$ is a parameter of the analyte and of the surrounding medium. For proteins with a RI commonly near 1.57, detection in water (RI = 1.33) yields a typical ΔRI of 0.24. By drying the samples and taking measurements in air (RI = 1.00), ΔRI can be increased to 0.57. Thus, a factor of 2.4 improvement in MDL is possible through this method. We note that this approach would preclude real-time detection and require further processing steps of the sample, which detracts from the strength of label-free detection. However, this drying methodology has been successfully utilized by Van Duyne and co-workers.[16]

The total sensing volume V_S of the nanoparticle is determined by the nanoparticle shape and decay length l_d. Smaller V_S and l_d are indicative of nanostructures with small, intense electric field enhancements. In general, the sensing volume will vary proportionally with the cube of the decay length simply because it is a three-dimensional volume subtended by the decay length. In the case of rods, smaller rods have shorter decay lengths. So ideally, one would want to use the smallest nanorods possible. However, smaller rods also exhibit smaller scattering cross sections C_{sca}, which means they scatter less light under dark-field illumination. For rods in particular, C_{sca} varies approximately as the square of the rod length and proportionately to rod diameter.[51] So if the length and diameter of a nanorod were both reduced by a factor of 2, C_{sca} would be reduced by about a factor of 8. On the other hand, to maintain an adequate SNR of the collected spectra, the intensity of the illumination source must be increased. An upper limit to this intensity exists because at some point the nanorods will melt due to photothermal effects.[70,71] The use of a broadband illumination source, such as a supercontinuum fiber laser, would allow the complete scattering spectrum to be collected and would provide a light output that is 6−10-fold more intense than the tungsten filament used in the experimental setup used here. Hence, eq 10 predicts that a physically realistic increase in illumination intensity by a factor of 10 could enable the visualization of smaller nanorods, effectively reducing the size of observable nanorods by about 1.5, thereby reducing the sensing volume and decay length, which would ultimately reduce the MDL by a factor of 7.

The decay length of the electric field enhancement l_d is determined by the geometry of the nanoparticles. Equation 10 assumes a uniform decay length for nanorods. The actual electric field enhancement has a more complicated geometry and, in particular, has been shown to exhibit larger enhancements near the ends of the rod.[30,55,72] Thus, analyte molecules that bind near the end of the nanorod will cause a greater LSPR shift than those binding on the lateral portion. For this reason, eq 10 is applicable to a MDL that stems from the LSPR response of individual biomolecules that are spatially averaged around the nanorod surface. It is reasonable to make this approximation for the experiments described here because the streptavidin molecules are adsorbed a fixed distance r from the nanorod surface, but no further spatial localization is possible. It has been shown through finite element modeling that the ends of nanorods exhibit much higher field enhancement than the spatial average.[73] Thus, if analyte binding can be limited to only within these regions, it is reasonable to assume a concurrent sensitivity increase greater than a factor of 10 due to the reduction of sensing volume. Some recent reports offer compelling end-to-end assembly of nanorods,[74] which could soon provide a route to site-specific functionalization of nanorods.

The binding distance r is the physical distance that the analyte binds from the surface of the nanoparticle. It is determined by the length of the receptor, which is approximated to be 2.4 nm for the experiments presented herein. EDC-NHS coupling is used to conjugate amine-terminated biotin to the carboxyl-terminated monolayer applied to the gold surface. We employ this binding moiety because it offers easy translation to other amine-terminated receptors, such as antibodies or aptamers.[36] It would be possible to employ a physically shorter receptor that would cause the target analyte to bind closer to the surface of the nanoparticle where the field enhancement, and thus RI sensitivity, is greater. For example, using thiol-terminated biotin has been successfully employed as a receptor for streptavidin detection with single nanoparticles.[75] This would reduce r by as much as a factor of 2, which in return reduces the overall MDL by a factor of $\exp(l_d^{-1})$. For the case of nanorods with decay length l_d generally on the order of 10−20 nm, this results in a factor of 1.1 improvement (*i.e.*, 10% decrease in MDL). In most practical situations, however, the size of the receptor−analyte pair is likely to be significantly larger than the model biotin−streptavidin pair used here (*e.g.*, antibody−protein), so that some of the gains realized from the optimization of the parameters discussed here are likely to be offset by the size of the receptor−

analyte pair. Nevertheless, these results suggest that minimizing the size of the receptor while retaining high binding affinity and specificity for its analyte is an important factor in extracting the minimum MDL of which LSPR sensors are capable. In this regard, the use of smaller receptors such as aptamers or smaller, engineered antibody fragments such as single chain antibodies are preferable to intact antibodies, which to date are the most commonly used class of receptors in biosensors.

The bulk RI sensitivity of a nanostructure S_0 is dependent on its size, shape, and material composition. However, Miller and Lazarides have observed that S_0 is correlated with the LSPR peak wavelength, regardless of nanoparticle shape.[60,61] Thus, for a nanostructure of known material composition, its bulk RI sensitivity can be predicted simply by characterizing its LSPR peak. Because longer wavelength resonances exhibit higher bulk RI sensitivities, the highest sensitivities will be from particles with LSPR peaks in the red end of the spectrum. Assuming the detection is to remain in the visible light spectrum, LSPR peaks at wavelengths up to 800 nm could be measured. Thus, bulk RI sensitivities as high as 600 nm/RIU could be expected. This is more than a two-fold improvement over the 260 nm/RIU sensitivity of nanorods used in this study. However, it is worth noting that, for the case of nanorods, longer resonances correspond to larger rods with larger sensing volumes and longer decay lengths. Equation 10 was used to balance the contributions for these effects to optimize sensor performance using the nanorod geometry. Thus, for this factor of 2 increase to be realistic, an alternative nanoparticle geometry would be sought that could indeed have a resonance far into the red without such large geometries. Additional sensitivity could be achieved by structuring the sensor to operate in near-IR wavelengths where the bulk RI sensitivities are higher, although the optics and instrumentation could be potentially more challenging. Also, silver nanoparticles exhibit sensitivities typically 1.5-fold higher than gold particles at similar resonant wavelengths. However, as mentioned above, the high reactivity of silver makes it less suitable as a sensor for use in biologically relevant media.

The peak measurement uncertainties U_{fit} and U_{system} represent the most direct way at improving sensor detection limits. Obviously, the smaller the wavelength shifts that can be reliably detected, the greater the accuracy and lower the overall MDL will be. For the system used in these experiments, U_{fit} was found to be approximately 0.02 nm while U_{system} was found to be 0.3 nm. Thus, the contribution to MDL is dominated by U_{system}, whereas U_{fit} acts more as an absolute limit for noise levels as discussed above. We performed an in-depth analysis of the contributing factors to U_{system} and found that a large portion of the uncertainty is the result of physical system stability.[49] In particular, it was found that stability in microscope focus and sample stage drift account for the largest contributions in uncertainty. It is proposed that, by using active feedback hardware to control microscope focus and XY-sample location, U_{system} can be reduced to the order of 0.005 nm.[49] Thus, the total uncertainty would then be dominated by U_{fit} resulting in a 15-fold decrease in MDL.

TABLE 1. Theoretical Improvement Factors That Can Reduce the Molecular Detection Limit of a Label-Free, Single Particle LSPR Sensor Based on the Modulation of Parameters from Equation 10

technique summary	variable from eq 10 involved	potential enhancement factor
drying	ΔRI	2.4
brighter illumination source	C_{sca}, V_s, and I_d	7
shorter binding moiety	r	1.1
LSPR peaks in IR	S_0	2
silver nanoparticles	S_0	1.5
high spectral resolution detection system	U_{system}	15
	total	~800

These possible enhancement factors are displayed in Table 1. From here, we see that the estimated possible enhancement factors could potentially provide an 800-fold improvement over the 18 molecule detection limit described herein. Thus, we show that the ultimate limit of label-free detection of single molecule binding events is theoretically possible within the framework of eq 10.

In conclusion, we have presented a simple mathematical model that analytically relates physical detection parameters of a single nanoparticle LSPR sensor to the minimum number of detectable analyte molecules. The utility of this model is two-fold. It can be used to select the optimum nanoparticle geometry for a desired detection system completely analytically, forgoing otherwise necessary comprehensive, experimental characterization. The minimum number of detectable molecules can be estimated as well as the number of molecules detected at saturation, which provides insight into the dynamic range of the system. Additionally, the model provides a framework through which the effects of potential system improvements can be assessed. Analysis of the theoretical limits of the dependent variables of eq 10 indicates that an 800-fold reduction of the MDL for the detection system described herein is possible. Clearly, not all of these potential avenues for MDL reduction can be realized concurrently. However, because our current MDL is 18 streptavidin molecules, we propose it is theoretically possible to design a system capable of detecting single molecule binding events by careful optimization of system parameters, as described herein.

EXPERIMENTAL SECTION

Materials. Hydrogen tetrachloroaurate trihydrate ($HAuCl_4$), sodium borohydride, ascorbic acid, phosphate buffered saline (PBS) tablets, poly(allylamine hydrochloride) (PAH), poly(4-styrenesulfonate, sodium salt) (PSS), silver nitrate, and mercaptohexadecanoic acid (MHA) were purchased from Sigma. Glass coverslips, ethanol, methanol, sodium chloride (NaCl), and hydrochloric acid (HCl) were purchased from VWR. Cetyltrimethylammonium bromide (CTAB) was purchased from Fluka. (+)-Biotinyl-3,6,9-trioxaundecanediamine (biotin−amine), 1-ethyl-3-(3-dimethylaminopropyl)carbodiimide (EDC), *N*-hydroxysuccinimide (NHS), and streptavidin were purchased from Pierce. Mercaptopropyltriethoxysilane (MPTES) was purchased from Gelest. (1-Mercaptoundec-11-yl)tri(ethylene glycol) (EG_3SH) was purchased from Prochimia. Distilled water purified by a reverse-osmosis filtration system (18 MΩ · cm, PureFlow Inc.) was used for all experiments.

Nanorod Synthesis. Gold nanorods were chemically synthesized by a seed-mediated growth procedure[34,76] similar to that described previously.[19,36] Spherical gold seed particles were prepared as follows: to a mixture of 7.5 mL of 0.1 M CTAB in water and 0.250 mL of 0.01 M $HAuCl_4$ was added under vigorous stirring 0.6 mL of chilled 0.01 M $NaBH_4$. The brown suspension was then gently heated and stirred for a few minutes. Gold nanorods were synthesized in a water bath at 29 °C as follows. To 95 mL of 0.1 M CTAB in water were added 0.6 mL of silver nitrate and 0.64 mL of 0.1 M ascorbic acid. The mixture was swirled after the addition of each reagent to ensure mixing. Sixty microliters of gold seed particles was added, and the mixture was inverted and allowed to sit overnight, resulting in a purple-colored suspension of gold nanorods. Excess CTAB was removed from the gold rod suspension by centrifugation twice at 4500 rpm for 30 min. The gold nanorods were resuspended in water to a total volume of 10 mL and stored at room temperature until further use.

Polyelectrolyte Deposition. Number 1 thickness rectangular 9 × 26 mm coverglasses were cleaned *via* the same method reported previously by Nath *et al.* for producing nanosphere biosensor chips.[15] First, they were cleaned by sonication for 20 min in a 1:1 HCl/methanol mixture. Then the coverglasses were rinsed with water and ethanol and then dried overnight at 65 °C. They were then incubated in a solution of 10% (v/v) MPTES in ethanol for 15 min followed by rinsing in ethanol and drying at 120 °C for 3 h. The coverglasses were incubated in the nanorod suspension overnight to ensure optimal coverage. The resulting nanorod-covered substrates were immersed in a solution of PAH (0.003 monomol/L in 1 M NaCl) for 30 min, rinsed with water, rinsed with 1 M NaCl, then immersed in a solution of PSS (0.003 monomol/L in 1 M NaCl). This procedure was repeated 13 times to deposit a total of 26 polymer layers. Each polyelectrolyte layer deposited is approximately 2 nm thick and has a RI of 1.52.[14,77,78] Between each polymer incubation step, an extinction spectrum was collected with a Varian Cary 300Bio UV−visible spectrophotometer. In this manner, plots were generated of λ* *versus* adsorbed layer thickness for two samples from each of the four different geometries for a total of eight plots. These eight plots were then used as the basis for the determination of $S(r)$.

Single Particle Detection. Scattering spectra were collected from individual nanorods using the Zeiss Axiovert 200 (Plan Neofluor 100X objective) dark-field illumination microspectroscopy system described previously.[19,50] Scattering spectra of individual nanorods were collected by imaging the microscope field of view to a line-imaging spectrometer (Acton Research SpectraPro 2150i). Streptavidin detection experiments with single gold nanorods were also performed as previously reported.[19] Briefly, the nanorods were immobilized onto 25 mm diameter, round No.1 glass coverslips, which were cleaned and incubated in MPTES as described above. The nanorod suspension was diluted in water to 1:15 (v/v), and then a 20 μL aliquot of the suspension was pipetted onto the center of the coverglass and immediately rinsed off with water. The nanorods were then modified by immersion of the chip in an ethanol solution of 0.5 mM EG_3SH and 0.5 mM MHA. The EG_3SH molecules of the mixed monolayer serve two purposes. They prevent nonspecific adsorption as well as modulate the surface density of the MHA molecules and hence of biotin that is subsequently chemically conjugated to the −COOH groups. Biotin was conjugated to the nanorods by incubating the SAM-functionalized nanorods in an aqueous solution of 0.4 M EDC and 0.1 M NHS for 7 min to convert the COOH groups to NHS esters. The chips were rinsed with water and were then immediately incubated in biotin−amine for 2 h and rinsed with water again. Streptavidin binding was performed by incubating the biotin-functionalized nanorods with a continuous flow of a streptavidin solution in PBS for 2 h. LSPR shifts were measured as the difference between the λ* of fits to the measured scattering spectra. To ensure the observed LSPR shifts resulted from specific interaction between biotin and streptavidin, controls for the binding experiments were performed by incubating biotin-functionalized gold nanorods in streptavidin solution that had been presaturated with excess (1 mM) free biotin.[19]

Acknowledgment. This work was supported by a grant from the Centers for Disease Control (NCID; R01 CI-00097) to A.C. G.J.N. acknowledges the support of a graduate fellowship from the NIH through a Biotechnology training grant (GM8555) awarded to the Center of Biomolecular and Tissue Engineering at Duke University. The authors also wish to thank the anonymous reviewers for their constructive suggestions that, we believe, helped improve this paper.

Supporting Information Available: An in-depth derivation of the distance dependence of nanoparticle sensitivity to local refractive index is available. This material is available free of charge *via* the Internet at http://pubs.acs.org.

REFERENCES AND NOTES

1. Yguerabide, J.; Yguerabide, E. E. Light-Scattering Submicroscopic Particles as Highly Fluorescent Analogs and Their Use as Tracer Labels in Clinical and Biological Applications. Ii. Experimental Characterization. *Anal. Biochem.* **1998**, *262*, 157–176.
2. Alivisatos, P. The Use of Nanocrystals in Biological Detection. *Nat. Biotechnol.* **2004**, *22*, 47–52.
3. Penn, S. G.; He, L.; Natan, M. J. Nanoparticles for Bioanalysis. *Curr. Opin. Chem. Biol.* **2003**, *7*, 609–615.
4. Iqbal, S. S.; Mayo, M. W.; Bruno, J. G.; Bronk, B. V.; Batt, C. A.; Chambers, J. P. A Review of Molecular Recognition Technologies for Detection of Biological Threat Agents. *Biosens. Bioelectron.* **2000**, *15*, 549–578.
5. Mirkin, C. A.; Ivanisevic, A.; Taton, T. A.; Letsinger, R. L.; Viswanadham, G. PCR-Less Detection of Genomic DNA with Nanoparticle Probes. *Abstracts of Papers*; American Chemical Society: Washington, DC, 2001; Vol. 222, p U578.
6. Schultz, D. A.; Mock, J. J.; Schultz, S.; Smith, D. R. Single-Target Molecule Detection with Nonbleaching Multicolor Optical Immunolabels. *Proc. Natl. Acad. Sci. U.S.A.* **2000**, *97*, 996–1001.
7. Mie, G. Beiträge Zur Optik Trüber Medien, Speziell Kolloidaler Metallösungen. *Ann. Phys.* **1908**, *25*, 377–445.
8. Yguerabide, J.; Yguerabide, E. E. Light-Scattering Submicroscopic Particles as Highly Fluorescent Analogs and Their Use as Tracer Labels in Clinical and Biological Applications. I. Theory. *Anal. Biochem.* **1998**, *262*, 137–156.
9. Kelly, K. L.; Coronado, E.; Zhao, L. L.; Schatz, G. C. The Optical Properties of Metal Nanoparticles: The Influence of Size, Shape, and Dielectric Environment. *J. Phys. Chem. B* **2003**, *107*, 668–677.
10. Khlebtsov, N. G.; Trachuk, L. A.; Mel'nikov, A. G. The Effect of the Size, Shape, and Structure of Metal Nanoparticles on the Dependence of Their Optical Properties on the Refractive Index of a Disperse Medium. *Opt. Spectrosc.* **2005**, *98*, 77–83.
11. Mock, J. J.; Barbic, M.; Smith, D. R.; Schultz, D. A.; Schultz, S. Shape Effects in Plasmon Resonance of Individual Colloidal Silver Nanoparticles. *J. Chem. Phys.* **2002**, *116*.
12. Mock, J. J.; Smith, D. R.; Schultz, S. Local Refractive Index Dependence of Plasmon Resonance Spectra from Individual Nanoparticles. *Nano Lett.* **2003**, *3*, 485–491.
13. Englebienne, P. Use of Colloidal Gold Surface Plasmon Resonance Peak Shift to Infer Affinity Constants from the

Interactions between Protein Antigens and Antibodies Specific for Single or Multiple Epitopes. *Analyst* **1998**, *123*, 1599–1603.
14. Nath, N.; Chilkoti, A. Label Free Colorimetric Biosensing Using Nanoparticles. *J. Fluoresc.* **2004**, *14*, 377–389.
15. Nath, N.; Chilkoti, A. A Colorimetric Gold Nanoparticle Sensor to Interrogate Biomolecular Interactions in Real Time on a Surface. *Anal. Chem.* **2002**, *74*, 504–509.
16. Haes, A. J.; Stuart, D. A.; Nie, S. M.; Van Duyne, R. P. Using Solution-Phase Nanoparticles, Surface-Confined Nanoparticle Arrays and Single Nanoparticles as Biological Sensing Platforms. *J. Fluoresc.* **2004**, *14*, 355–367.
17. Frederix, F.; Friedt, J. M.; Choi, K. H.; Laureyn, W.; Campitelli, A.; Mondelaers, D.; Maes, G.; Borghs, G. Biosensing Based on Light Absorption of Nanoscaled Gold and Silver Particles. *Anal. Chem.* **2003**, *75*, 6894–6900.
18. Dahlin, A.; Zach, M.; Rindzevicius, T.; Kall, M.; Sutherland, D. S.; Hook, F. Localized Surface Plasmon Resonance Sensing of Lipid-Membrane-Mediated Biorecognition Events. *J. Am. Chem. Soc.* **2005**, *127*, 5043–5048.
19. Nusz, G. J.; Marinakos, S. M.; Curry, A. C.; Dahlin, A.; Höök, F.; Wax, A.; Chilkoti, A. Label-Free Plasmonic Detection of Biomolecular Binding by a Single Gold Nanorod. *Anal. Chem.* **2008**, *80*, 984–989.
20. Raschke, G.; Kowarik, S.; Franzl, T.; Sonnichsen, C.; Klar, T. A.; Feldmann, J.; Nichtl, A.; Kurzinger, K. Biomolecular Recognition Based on Single Gold Nanoparticle Light Scattering. *Nano Lett.* **2003**, *3*, 935–938.
21. McFarland, A. D.; Van Duyne, R. P. Single Silver Nanoparticles as Real-Time Optical Sensors with Zeptomole Sensitivity. *Nano Lett.* **2003**, *3*, 1057–1062.
22. Rindzevicius, T.; Alaverdyan, Y.; Dahlin, A.; Hook, F.; Sutherland, D. S.; Kall, M. Plasmonic Sensing Characteristics of Single Nanometric Holes. *Nano Lett.* **2005**, *5*, 2335–2339.
23. Sherry, L. J.; Jin, R. C.; Mirkin, C. A.; Schatz, G. C.; Van Duyne, R. P. Localized Surface Plasmon Resonance Spectroscopy of Single Silver Triangular Nanoprisms. *Nano Lett.* **2006**, *6*, 2060–2065.
24. van Dijk, M. A.; Lippitz, M.; Orrit, M. Far-Field Optical Microscopy of Single Metal Nanoparticles. *Acc. Chem. Res.* **2005**, *38*, 594–601.
25. Sonnichsen, C.; Geier, S.; Hecker, N. E.; von Plessen, G.; Feldmann, J.; Ditlbacher, H.; Lamprecht, B.; Krenn, J. R.; Aussenegg, F. R.; Chan, V. Z. H.; Spatz, J. P.; Moller, M. Spectroscopy of Single Metallic Nanoparticles Using Total Internal Reflection Microscopy. *Appl. Phys. Lett.* **2000**, *77*, 2949–2951.
26. Haes, A. J.; Van Duyne, R. P.; Zou, S. L.; Schatz, G. C. Nanoscale Optical Biosensor: Short Range Distance Dependence of the Localized Surface Plasmon Resonance of Noble Metal Nanoparticles. *J. Phys. Chem. B* **2004**, *108*, 6961–6968.
27. Haes, A. J.; Van Duyne, R. P.; Zou, S. L.; Schatz, G. C. A Nanoscale Optical Biosensor: The Long Range Distance Dependence of the Localized Surface Plasmon Resonance of Noble Metal Nanoparticles. *J. Phys. Chem. B* **2004**, *108*, 109–116.
28. Evanoff, D. D.; White, R. L.; Chumanov, G. Measuring the Distance Dependence of the Local Electromagnetic Field from Silver Nanoparticles. *J. Phys. Chem. B* **2004**, *108*, 1522–1524.
29. Hao, E.; Schatz, G. C. Electromagnetic Fields around Silver Nanoparticles and Dimers. *J. Chem. Phys.* **2004**, *120*, 357–366.
30. Imura, K.; Okamoto, H.; Nagahra, T. Plasmon Mode Imaging of Single Gold Nanorods. *J. Am. Chem. Soc.* **2004**, *126*, 12730–12731.
31. Stenberg, E.; Persson, B.; Roos, H.; Urbaniczky, C. Quantitative Determination of Surface Concentration of Protein with Surface Plasmon Resonance Using Radiolabeled Proteins. *J. Colloid Interface Sci.* **1991**, *143*, 513–526.
32. Vollmer, F.; Braun, D.; Libchaber, A.; Khoshsima, M.; Teraoka, I.; Arnold, S. Protein Detection by Optical Shift of a Resonant Microcavity. *Appl. Phys. Lett.* **2002**, *80*, 4057–4059.
33. Chumanov, G.; Sokolov, K.; Gregory, B. W.; Cotton, T. M. Colloidal Metal Films as a Substrate for Surface-Enhanced Spectroscopy. *J. Phys. Chem.* **1995**, *99*, 9466–9471.
34. Nikoobakht, B.; El-Sayed, M. A. Preparation and Growth Mechanism of Gold Nanorods (NRs) Using Seed-Mediated Growth Method. *Chem. Mater.* **2003**, *15*, 1957–1962.
35. Chen, C.-D.; Cheng, S.-F.; Chau, L.-K.; Wang, C. R. C. Sensing Capability of the Localized Surface Plasmon Resonance of Gold Nanorods. *Biosens. Bioelectron.* **2007**, *22*, 926–932.
36. Marinakos, S. M.; Chen, S.; Chilkoti, A. Plasmonic Detection of a Model Analyte in Serum by a Gold Nanorod Sensor. *Anal. Chem.* **2007**, *79*, 5278–5283.
37. Jana, N. R.; Gearheart, L.; Murphy, C. J. Wet Chemical Synthesis of High Aspect Ratio Cylindrical Gold Nanorods. *J. Phys. Chem. B* **2001**, *105*, 4065–4067.
38. Busbee, B. D.; Obare, S. O.; Murphy, C. J. An Improved Synthesis of High-Aspect-Ratio Gold Nanorods. *Adv. Mater.* **2003**, *15*, 414–416.
39. Sau, T. K.; Murphy, C. J. Room Temperature, High-Yield Synthesis of Multiple Shapes of Gold Nanoparticles in Aqueous Solution. *J. Am. Chem. Soc.* **2004**, *126*, 8648–8649.
40. Link, S.; Mohamed, M. B.; El-Sayed, M. A. Simulation of the Optical Absorption Spectra of Gold Nanorods as a Function of Their Aspect Ratio and the Effect of the Medium Dielectric Constant. *J. Phys. Chem. B* **1999**, *103*, 3073–3077.
41. Weissleder, R. A Clearer Vision for *In Vivo* Imaging. *Nat. Biotechnol.* **2001**, *19*, 316–317.
42. Jackson, J. B.; Westcott, S. L.; Hirsch, L. R.; West, J. L.; Halas, N. J. Controlling the Surface Enhanced Raman Effect *via* the Nanoshell Geometry. *Appl. Phys. Lett.* **2003**, *82*, 257–259.
43. Hanarp, P.; Kall, M.; Sutherland, D. S. Optical Properties of Short Range Ordered Arrays of Nanometer Gold Disks Prepared by Colloidal Lithography. *J. Phys. Chem. B* **2003**, *107*, 5768–5772.
44. Aizpurua, J.; Hanarp, P.; Sutherland, D. S.; Kall, M.; Bryant, G. W.; de Abajo, F. J. G. Optical Properties of Gold Nanorings. *Phys. Rev. Lett.* **2003**, *90*.
45. Raschke, G.; Brogl, S.; Susha, A. S.; Rogach, A. L.; Klar, T. A.; Feldmann, J.; Fieres, B.; Petkov, N.; Bein, T.; Nichtl, A.; Kurzinger, K. Gold Nanoshells Improve Single Nanoparticle Molecular Sensors. *Nano Lett.* **2004**, *4*, 1853–1857.
46. Hafner, J. H.; Nehl, C. L.; Grady, N. K.; Goodrich, G. P.; Tam, F.; Halas, N. J. Scattering Spectra of Single Gold Nanoshells. *Nano Lett.* **2004**, *4*, 2355–2359.
47. Novo, C.; Gomez, D.; Perez-Juste, J.; Zhang, Z. Y.; Petrova, H.; Reismann, M.; Mulvaney, P.; Hartland, G. V. Contributions from Radiation Damping and Surface Scattering to the Linewidth of the Longitudinal Plasmon Band of Gold Nanorods: A Single Particle Study. *Phys. Chem. Chem. Phys.* **2006**, *8*, 3540–3546.
48. Prescott, S. W.; Mulvaney, P. Gold Nanorod Extinction Spectra. *J. Appl. Phys.* **2006**, *99*.
49. Curry, A.; Nusz, G.; Chilkoti, A.; Wax, A. Analysis of Total Uncertainty in Spectral Peak Measurements for Plasmonic Nanoparticle-Based Biosensors. *Appl. Opt.* **2007**, *46*, 1931–1939.
50. Curry, A.; Nusz, G.; Chilkoti, A.; Wax, A. Substrate Effect on Refractive Index Dependence of Plasmon Resonance for Individual Silver Nanoparticles Observed Using Darkfield Micro-Spectroscopy. *Opt. Express* **2005**, *13*, 2668–2677.
51. Kuwata, H.; Tamaru, H.; Esumi, K.; Miyano, K. Resonant Light Scattering from Metal Nanoparticles: Practical Analysis Beyond Rayleigh Approximation. *Appl. Phys. Lett.* **2003**, *83*, 4625–4627.
52. Xu, X. D.; Cortie, M. B. Shape Change and Color Gamut in Gold Nanorods, Dumbbells, and Dog Bones. *Adv. Funct. Mater.* **2006**, *16*, 2170–2176.
53. Yan, B. H.; Yang, Y.; Wang, Y. C. Comment On "Simulation of the Optical Absorption Spectra of Gold Nanorods as a

Function of Their Aspect Ratio and the Effect of the Medium Dielectric Constant". *J. Phys. Chem. B* **2003**, *107*, 9159.
54. Link, S.; El-Sayed, M. A.; Mohamed, M. B. Simulation of the Optical Absorption Spectra of Gold Nanorods as a Function of Their Aspect Ratio and the Effect of the Medium Dielectric Constant (Vol 103b, Pg 3073, 1999). *J. Phys. Chem. B* **2005**, *109*, 10531–10532.
55. Link, S.; Mohamed, M. B.; El-Sayed, M. A. Simulation of the Optical Absorption Spectra of Gold Nanorods as a Function of Their Aspect Ratio and the Effect of the Medium Dielectric Constant. *J. Phys. Chem. B* **1999**, *103*, 3073–3077.
56. Nath, N.; Chilkoti, A. Label-Free Biosensing by Surface Plasmon Resonance of Nanoparticles on Glass: Optimization of Nanoparticle Size. *Anal. Chem.* **2004**, *76*, 5370–5378.
57. Whitney, A. V.; Elam, J. W.; Zou, S. L.; Zinovev, A. V.; Stair, P. C.; Schatz, G. C.; Van Duyne, R. P. Localized Surface Plasmon Resonance Nanosensor: A High-Resolution Distance-Dependence Study Using Atomic Layer Deposition. *J. Phys. Chem. B* **2005**, *109*, 20522–20528.
58. Hicks, E. M.; Zhang, X. Y.; Zou, S. L.; Lyandres, O.; Spears, K. G.; Schatz, G. C.; Van Duyne, R. P. Plasmonic Properties of Film over Nanowell Surfaces Fabricated by Nanosphere Lithography. *J. Phys. Chem. B* **2005**, *109*, 22351–22358.
59. Haes, A. J.; Van Duyne, R. P. A Nanoscale Optical Biosensor: Sensitivity and Selectivity of an Approach Based on the Localized Surface Plasmon Resonance Spectroscopy of Triangular Silver Nanoparticles. *J. Am. Chem. Soc.* **2002**, *124*, 10596–10604.
60. Miller, M. M.; Lazarides, A. A. Sensitivity of Metal Nanoparticle Plasmon Resonance Band Position to the Dielectric Environment as Observed in Scattering. *J. Opt. A: Pure Appl. Opt.* **2006**, *8*, S239–S249.
61. Miller, M. M.; Lazarides, A. A. Sensitivity of Metal Nanoparticle Surface Plasmon Resonance to the Dielectric Environment. *J. Phys. Chem. B* **2005**, *109*, 21556–21565.
62. Neish, C. S.; Martin, I. L.; Henderson, R. M.; Edwardson, J. M. Direct Visualization of Ligand-Protein Interactions Using Atomic Force Microscopy. *Br. J. Pharmacol.* **2002**, *135*, 1943–1950.
63. Jung, L. S.; Campbell, C. T.; Chinowsky, T. M.; Mar, M. N.; Yee, S. S. Quantitative Interpretation of the Response of Surface Plasmon Resonance Sensors to Adsorbed Films. *Langmuir* **1998**, *14*, 5636–5648.
64. Chien, F. C.; Chen, S. J. Direct Determination of the Refractive Index and Thickness of a Biolayer Based on Coupled Waveguide-Surface Plasmon Resonance Mode. *Opt. Lett.* **2006**, *31*, 187–189.
65. Weber, P. C.; Ohlendorf, D. H.; Wendoloski, J. J.; Salemme, F. R. Structural Origins of High-Affinity Biotin Binding to Streptavidin. *Science* **1989**, *243*, 85–88.
66. Hendrickson, W. A.; Pahler, A.; Smith, J. L.; Satow, Y.; Merritt, E. A.; Phizackerley, R. P. Crystal-Structure of Core Streptavidin Determined from Multiwavelength Anomalous Diffraction of Synchrotron Radiation. *Proc. Natl. Acad. Sci. U.S.A.* **1989**, *86*, 2190–2194.
67. Hinrichsen, E. L.; Feder, J.; Jossang, T. Geometry of Random Sequential Adsorption. *J. Stat. Phys.* **1986**, *44*, 793–827.
68. Jung, L. S.; Nelson, K. E.; Stayton, P. S.; Campbell, C. T. Binding and Dissociation Kinetics of Wild-Type and Mutant Streptavidins on Mixed Biotin-Containing Alkylthiolate Monolayers. *Langmuir* **2000**, *16*, 9421–9432.
69. Kim, Y. P.; Hong, M. Y.; Kim, J.; Oh, E.; Shon, H. K.; Moon, D. W.; Kim, H. S.; Lee, T. G. Quantitative Analysis of Surface-Immobilized Protein by Tof-Sims: Effects of Protein Orientation and Trehalose Additive. *Anal. Chem.* **2007**, *79*, 1377–1385.
70. Link, S.; El-Sayed, M. A. Spectroscopic Determination of the Melting Energy of a Gold Nanorod. *J. Chem. Phys.* **2001**, *114*, 2362–2368.
71. Chang, S. S.; Shih, C. W.; Chen, C. D.; Lai, W. C.; Wang, C. R. C. The Shape Transition of Gold Nanorods. *Langmuir* **1999**, *15*, 701–709.
72. Link, S.; El-Sayed, M. A. Spectral Properties and Relaxation Dynamics of Surface Plasmon Electronic Oscillations in Gold and Silver Nanodots and Nanorods. *J. Phys. Chem. B* **1999**, *103*, 8410–8426.
73. Muskens, O. L.; Bachelier, G.; Del Fatti, N.; Vallee, F.; Brioude, A.; Jiang, X. C.; Pileni, M. P. Quantitative Absorption Spectroscopy of a Single Gold Nanorod. *J. Phys. Chem. C* **2008**, *112*, 8917–8921.
74. Park, H. S.; Agarwal, A.; Kotov, N. A.; Lavrentovich, O. D. Controllable Side-by-Side and End-to-End Assembly of Au Nanorods by Lyotropic Chromonic Materials. *Langmuir* **2008**, *24*, 13833–13837.
75. Dahlin, A. B.; Tegenfeldt, J. O.; Hook, F. Improving the Instrumental Resolution of Sensors Based on Localized Surface Plasmon Resonance. *Anal. Chem.* **2006**, *78*, 4416–4423.
76. Jana, N. R.; Gearheart, L.; Murphy, C. J. Seed-Mediated Growth Approach for Shape-Controlled Synthesis of Spheroidal and Rod-Like Gold Nanoparticles Using a Surfactant Template. *Adv. Mater.* **2001**, *13*, 1389–1393.
77. Caruso, F.; Lichtenfeld, H.; Giersig, M.; Mohwald, H. Electrostatic Self-Assembly of Silica Nanoparticle-Polyelectrolyte Multilayers on Polystyrene Latex Particles. *J. Am. Chem. Soc.* **1998**, *120*, 8523–8524.
78. Buscher, K.; Graf, K.; Ahrens, H.; Helm, C. A. Influence of Adsorption Conditions on the Structure of Polyelectrolyte Multilayers. *Langmuir* **2002**, *18*, 3585–3591.